Int. J. Heat Mass Transfer. Vol. 29, No. 4, pp. 573–592, 1986
Printed in Great Britain

0017–9310/86 $3.00 + 0.00

Numerical simulation of buoyant, turbulent flow—I. Free convection along a heated, vertical, flat plate

W. M. TO and J. A. C. HUMPHREY
Department of Mechanical Engineering, University of California, Berkeley, CA 94720, U.S.A.

(*Received* 4 *February* 1985 *and in final form* 30 *October* 1985)

Abstract—Two models have been developed for predicting free convection low Reynolds number turbulent flows. The models also apply to mixed convection flows. The first, a k–ε model, is based on the notion of eddy diffusivities for momentum and heat. The second, an algebraic stress model, is based on approximations derived for the anisotropic turbulent fluxes by a suitable truncation of their conservation equations. Both formulations apply to variable property flows with high overheat ratios, $\Delta T/T_\infty$, and have not required the definition of new model constants. No attempt has been made to modify previously established values of the constants in order to improve agreement between measurements and predictions of the flow investigated. Such an optimization must await the availability of more detailed and reliable experimental measurements of turbulence-related quantities.

Fully elliptic forms of the differential transport equations, subject to appropriately specified boundary conditions, have been solved numerically for two flow configurations. Both are two-dimensional. The first corresponds to free convection along a heated vertical flat plate and is the subject of Part I of this study. The second corresponds to free and mixed convection from a heated cavity of arbitrary rectangular cross-section and variable orientation, and is the subject of Part II.

For the case of the vertical plate, a comparison between measurements and predictions shows that both models yield fairly accurate results for the mean flow and heat transfer. Near-wall velocity and temperature distributions predicted by both models reveal the 1/3 power-law dependence derived by George and Capp [*Int. J. Heat Mass Transfer* **22**, 813–826 (1979)] and confirmed for temperature by Siebers *et al* [*J. Heat Transfer* **107**, 124–132 (1985)]. Values of the constants in the power-law relations for velocity and temperature have been obtained here numerically for high and low $\Delta T/T_\infty$. Predictions of the anisotropic Reynolds stress and turbulent heat flux distributions are in good qualitative agreement with the measurements of Miyamoto *et al.* [*Proc. 7th Int. Heat Transfer Conference*, Vol. 2, pp. 323–328 (1982)]. In particular, regions of negative buoyant and shear production of turbulent kinetic energy observed experimentally are clearly revealed by the calculations.

1. INTRODUCTION

1.1. *The problem of interest and objectives of this study*

ASIDE from its intrinsic value, the accurate modeling of turbulent free convection from a heated, flat plate is considered to be a logical first step towards the numerical simulation of more complex, buoyancy-affected, turbulent flows. However, in reviewing the literature it becomes apparent that even the case of steady, two-dimensional (in the mean) free convection along a vertical flat plate has not yet been satisfactorily resolved. While there exist numerous experimental measurements and theoretical calculations of mean flow and heat transfer quantities (such as velocity, temperature and the heat transfer coefficient), and there are empirically and theoretically derived correlations available to predict the heat transfer to within experimental uncertainty, no calculation to date has been directed towards resolving the mean flow and the anisotropic turbulence characteristics *simultaneously*. Furthermore, all calculation approaches so far have made use of the Boussinesq approximation, which limits their applicability to relatively small values of the overheat ratio, $(T_w - T_\infty)/T_\infty$.

The objective of the present study has been to develop and test two closure approximations which will correctly predict the mean flow and heat transfer of a variable property fluid in turbulent free convection along a heated, vertical, flat plate. The models also apply to mixed convection flows. In one case closure is based on the notion of isotropic eddy diffusion coefficients for the turbulent transport of momentum and heat, while in the other special attention is paid to simulating the anisotropic characteristics of the turbulent fluxes. Both models account for low Reynolds number turbulent flow conditions near walls, where wall-damping takes place, and far away from them where, in the absence of shear production, turbulent fluctuations decay to small values.

A comparison between the quantities predicted by both models show that they are equally capable of yielding fairly accurate results for the mean flow and heat transfer. As a result, the simpler model, that based on eddy diffusion coefficients, has also been applied to simulate free and mixed convection in strongly heated cavities. In this paper, Part I, we communicate the work performed for the flat plate configuration. In a second paper, Part II, we provide an account of the work performed for the cavity configuration.

1.2. *Earlier work*

(i) *Free convection along a vertical, flat plate.* A literature review of convective heat transfer in heated cavities, enclosures and along flat plates has been given

NOMENCLATURE

C_p specific heat at constant pressure
D turbulence quantity related to ε through $\nu, \overline{(\partial u_i'/\partial x_j)(\partial u_i'/\partial x_j)} = \varepsilon/\nu$
g gravitational constant
g_i component i of the gravitation vector
G buoyancy production of turbulent kinetic energy, $\overline{\rho' u_i'} g_i$
G_{ij} buoyancy production of $\overline{u_i' u_j'}$ (defined in text)
Gr_x local Grashof number, $g\beta_\infty \Delta T x^3/\nu_\infty^2$
Gr_x^* modified local Grashof number, $g\beta_\infty \dot{q}_w x^4/\gamma_\infty \nu_\infty^2$
h heat transfer coefficient
k turbulent kinetic energy, $\overline{u_i' u_i'}/2$
Nu_x local Nusselt number, hx/γ_∞
p pressure
P shear production of turbulent kinetic energy, $-\overline{\rho u_i' u_j'}\, \partial \bar{u}_i/\partial x_j$
P_{ij} shear production of $\overline{u_i' u_j'}$ (defined in text)
P_{iT} shear production of $\overline{u_i' T'}$ (defined in text)
Pr Prandtl number, $\mu C_p/\gamma$
Pr_t turbulent Prandtl number
$\dot{q}_w$ wall heat flux
Re_t turbulent Reynolds number, $\bar{\rho} k^2/\mu\varepsilon$
$R_{u'T'}$ velocity–temperature correlation coefficient, $\overline{u'T'}/\sqrt{(\overline{u'^2})}\sqrt{(\overline{T'^2})}$
T temperature
T_f film temperature, $(T_w + T_\infty)/2$
T_w wall temperature
T_∞ ambient temperature (293 K)
t time
u longitudinal (streamwise) velocity component
u_i velocity component in i-direction
$\bar{u}_m$ maximum velocity along a flat plate
u_b characteristic velocity along a flat plate, $2\sqrt{g\beta_\infty \Delta T x}$
u_T inner region velocity scale, $(g\beta_\infty \Delta T \nu_\infty/Pr)^{1/3}$
u^+ dimensionless velocity, $\bar{u}/u_\tau$
u_τ characteristic shear stress velocity, $\sqrt{\tau_w/\rho}$
$\overline{u'T'}$ longitudinal turbulent heat flux
$\overline{u'v'}$ turbulent shear stress
v transverse velocity component (perpendicular to flat plate)
$\overline{v'T'}$ transverse turbulent heat flux
w spanwise velocity component (parallel to flat plate)
x_i spatial coordinate in i-direction
x longitudinal coordinate; distance from the leading edge of a flat plate
y transverse coordinate; distance perpendicular to the flat plate
y^+ dimensionless transverse coordinate, y/y_τ
y_τ transverse length scale, ν/u_τ

Greek symbols

β coefficient of volume expansion, $1/T_\infty$
γ thermal conductivity
δ_{ij} Kronecker delta
δ_u outer region length scale, $\int_0^\infty (\bar{u}/\bar{u}_m)\, dy$
ΔT characteristic temperature difference, $T_w - T_\infty$
ε isotropic dissipation of turbulent kinetic energy, νD
ζ dimensionless transverse coordinate, yNu_x/x
η_T inner region length scale, $[(\nu_\infty/Pr)^2/(g\beta_\infty \Delta T)]^{1/3}$
η_T' modified inner region length scale, $\eta_T(\gamma_w/\gamma_\infty)(T_w/T_\infty)^{0.14}$
θ nondimensional temperature, $(T - T_\infty)/(T_w - T_\infty)$
μ molecular viscosity
μ_t turbulent viscosity
ν molecular kinematic viscosity
π_{ij} pressure redistribution of $\overline{u_i' u_j'}$
π_{iT} pressure redistribution of $\overline{u_i' T'}$
ρ density
σ_k Prandtl number for k
σ_ε Prandtl number for ε
τ_w wall shear stress.

Superscripts

$'$ fluctuating quantities
$\bar{}$ mean quantities.

Subscripts

i, j spatial coordinate indices
m maximum value
t turbulent quantity
w wall condition
f film temperature
∞ ambient condition.

in Humphrey *et al.* [1]. A summary is provided here of those investigations most relevant to the present work.

Among the early experimental works on turbulent free convection flow along vertical, flat plates are the contributions by Warner and Arpaci [2], Lock and Trotter [3], Goldstein and Eckert [4] and Cheesewright [5] for low overheat ratio. More recent investigations using the laser–Doppler velocimeter (LDV) technique have been conducted by Cheesewright and Ierokipiotis [6] for $\Delta T/T_\infty \sim 0.2$, by Cairnie and Harrison [7] for $0.26 < \Delta T/T_\infty < 1.28$ and by Miyamoto *et al.* [8] for $\Delta T/T_\infty \sim 0.12$. By measuring temperature and velocity simultaneously at essentially the same location, Miyamoto *et al.* [8] obtained turbulent stress and heat flux distributions in addition to mean flow quantities. Cheesewright and Doan [9] have performed a fairly detailed study of space–time correlations using the hot wire technique. Siebers *et al.* [10] have measured distributions of the heat transfer coefficient and of temperature over the Grashof number range $1.7 \times 10^{11} < Gr_x < 1.86 \times 10^{12}$ with $0.14 < \Delta T/T_\infty < 1.73$. A major result from their work was the following correlation for the local Nusselt number:

$$Nu_x = 0.098\ Gr_x^{1/3}\left(\frac{T_w}{T_\infty}\right)^{-0.14}. \qquad (1)$$

The last term in equation (1) accounts for the physical property dependence of air on temperature.

Theoretical analyses using integral formulations have been performed by, among others, Eckert and Jackson [11], Bayley [12], Oosthuizen [13] and Kato *et al.* [14]. Numerical predictions using isotropic eddy diffusion turbulence models have been made by Mason and Seban [15], Cecebi and Khattab [16] and Siebers [17]. Predictions based on the low Reynolds number k–ε turbulence model of Jones and Launder [18] have been made by Plumb and Kennedy [19] and Lin and Churchill [20]. The above theoretical analyses and numerical procedures have yielded results in good agreement with measurements of heat transfer. The numerical approaches also give correct distributions of mean velocity and temperature but, due to the assumption of an isotropic eddy diffusion coefficient, cannot predict the detailed anisotropic characteristics of the turbulent flow.

(ii) *Modeling turbulence with buoyant effects.* Theoretical formulations for simulating high Reynolds number turbulent flows subject to gravitational forces have been developed for conditions where the Boussinesq approximation applies; see, for example, the reviews given by Launder [21], Hirata *et al.* [22] and Hosain and Rodi [23]. For an elegant discussion of the Boussinesq approximation the reader is referred to Gray and Giorgini [24].

The present work builds upon and extends the investigations by Launder [25] and Gibson and Launder [26]. These authors have derived algebraic relations for the turbulent stress and heat flux components in high Reynolds number (locally isotropic) equilibrium shear flows. Launder [25] suggested a way for including gravitational effects in the pressure-correlation terms affecting the balance of the turbulent fluxes. Gibson and Launder [26] extended this work by accounting for the modification of the fluctuating pressure field by the presence of a wall. Applications of these concepts are to be found in the numerical studies of Gibson and Launder [27] and Ljuboja and Rodi [28].

In high Reynolds number turbulence model formulations it is possible to use logarithmic law-of-the-wall relations for velocity and temperature to patch the region of flow lying between a wall and the first calculation location adjacent to the wall. This is not possible in the present flow where low Reynolds number conditions arise both near the wall and far away from it. The formulation to be developed must account for this effect as well as arbitrary wall orientation and the variation of physical properties with temperature.

Velocity and temperature power-law relations have been derived by George and Capp [29] for the buoyant sublayer region of turbulent free convection along a heated, vertical, flat plate at low $\Delta T/T_\infty$. Siebers *et al.* [10] verified the 1/3 power dependence for temperature with distance from the wall, but they found it necessary to modify the inner region length scale proposed in ref. [29] by including a dimensionless wall temperature factor. This empirical adjustment is needed to account for the temperature dependence of physical properties at high overheat ratios.

For low $\Delta T/T_\infty$ it is possible to estimate values for the constants in the power-law relations of ref. [29] from existing measurements of temperature and recent detailed measurements of velocity. However, corresponding values of the constants for high $\Delta T/T_\infty$ can only be obtained for temperature, from the data of ref. [10]. Given that the relations derived [29] apply only to vertical plates, and given the relatively large uncertainties associated with determining the power-law constants, we have eschewed a modeling approach which relies on the availability of some general form of a wall relation. Instead, we have sought to predict the flow directly, by using a generalized model formulation which encompasses both high and low turbulence Reynolds number regions of the flow for arbitrary values of $\Delta T/T_\infty$ and wall orientation. Following this approach it is possible to compute detailed variations for temperature and velocity in the buoyant sublayer, from which (it will be shown) corresponding power-law relations can be derived.

2. NUMERICAL PROCEDURE

2.1. *Mean transport equations and auxiliary relations*

The starting point for the turbulence modeling effort is the system of transport equations given in LeQuere *et al.* [30] for variable physical property flows. The fluid of interest here, air, is presumed to be a perfect gas with

$Pr = 0.71$. Conservation equations for mass, momentum and energy, and a mean equation of state, are obtained by Reynolds decomposition of instantaneous quantities in the equations into the sum of the mean and fluctuating parts and averaging the result as shown in Appendix A of Humphrey *et al.* [31]. The result, ignoring fluctuations of physical properties except density, is:

$$\frac{\partial \bar{\rho}}{\partial t} + \frac{\partial}{\partial x_j}(\bar{\rho}\bar{u}_j + \overline{\rho' u_j'}) = 0 \tag{2}$$

$$\frac{\partial}{\partial t}(\bar{\rho}\bar{u}_i) + \frac{\partial}{\partial x_j}(\bar{\rho}\bar{u}_j\bar{u}_i) + \frac{\partial}{\partial t}(\overline{\rho' u_i'}) + \frac{\partial}{\partial x_j}(\overline{\rho' u_j' \bar{u}_i} + \overline{\rho' u_i' \bar{u}_j}) = -\frac{\partial \bar{p}}{\partial x_i} + (\bar{\rho} - \rho_\infty) g_i + \frac{\partial}{\partial x_j}\left[\mu\left(\frac{\partial \bar{u}_i}{\partial x_j} + \frac{\partial \bar{u}_j}{\partial x_i}\right) - \overline{\rho u_i' u_j'}\right] \tag{3}$$

$$\frac{\partial}{\partial x_j}(\bar{\rho}\bar{u}_j\bar{T} + \overline{\rho' u_j'}\bar{T} + \overline{\rho' T'}\bar{u}_j) = \frac{\partial}{\partial x_j}\left(\frac{\gamma}{C_p}\frac{\partial \bar{T}}{\partial x_j} - \overline{\rho u_j' T'}\right) \tag{4}$$

$$\bar{\rho}\bar{T} + \overline{\rho' T'} = \rho_\infty T_\infty. \tag{5}$$

An additional pair of useful relations can be obtained from the equation of state. They are:

$$\overline{\rho' u_i'}\bar{T} + \overline{\rho u_i' T'} = 0 \tag{6}$$

$$\overline{\rho' T'}\bar{T} + \overline{\rho T'^2} = 0. \tag{7}$$

Through these auxiliary relations $\overline{\rho' u_i'}$ and $\overline{\rho' T'}$ can be calculated using the models employed to approximate $\overline{\rho u_i' T'}$ and $\overline{\rho T'^2}$, respectively.

To close the above system of equations, assumptions concerning the mean flow dependence of $\overline{\rho u_i' u_j'}$, $\overline{\rho u_i' T'}$ and $\overline{\rho T'^2}$ must be made, or expressions for these quantities must be obtained from their respective transport equations. The former approach introduces the concept of a turbulent viscosity which is determined by k, the kinetic energy of turbulence and ε, its rate of isotropic dissipation. This model is commonly referred to as the k–ε model (KEM). The latter approach, in the case of 2-D flow, involves six partial differential equations for the turbulence correlations. Truncation of these transport equations, obtained by neglecting convection and diffusion terms, yields a system of algebraic equations relating the turbulent fluxes to known or calculable flow quantities; hence the terminology, algebraic stress model (ASM).

From here on, third and higher order correlations involving ρ' are neglected. This is done principally because at the present time there is insufficient information for developing good approximations for such terms. However, the omission of these terms is not expected to alter significantly the mean flow results. The effect of their omission on the calculated turbulence quantities is more difficult to ascertain but is also expected to be small.

2.2. *Two-equation model (KEM)*

Maintaining an analogy with laminar flow, the turbulent fluxes $\overline{\rho u_i' u_j'}$ and $\overline{\rho u_i' T'}$ are assumed to obey gradient type relations as follows,

$$-\overline{\rho u_i' u_j'} = \mu_t\left(\frac{\partial \bar{u}_i}{\partial x_j} + \frac{\partial \bar{u}_j}{\partial x_i}\right) - \frac{2}{3}\bar{\rho} k\, \delta_{ij} \tag{8}$$

$$-\overline{\rho u_i' T'} = \frac{\mu_t}{Pr_t}\frac{\partial \bar{T}}{\partial x_i}. \tag{9}$$

The turbulence viscosity, μ_t, is assumed to be proportional to a turbulence velocity scale and a turbulence length scale. In the limit of high Reynolds number, Jones and Launder [18] propose

$$\mu_t = C_\mu \bar{\rho}\frac{k^2}{\varepsilon}. \tag{10}$$

In this expression C_μ is a proportionality constant and ε is defined as

$$\varepsilon = \nu D = \nu\overline{\frac{\partial u_i'}{\partial x_j}\frac{\partial u_i'}{\partial x_j}}. \tag{11}$$

Exact transport equations for k and D† can be derived from the momentum equation as shown in ref. [31]. Simplified forms of the equations, obtained by neglecting third and higher order correlations involving ρ', correlations involving $\partial u_i'/\partial x_i$ and $\partial\rho/\partial x_j$, and variable viscosity property terms, are the basis for the model presented in detail in ref. [31].

In the model, a gradient assumption is used to approximate the diffusion of k and ε [18,32], with the pressure contribution to turbulent diffusion assumed to be negligibly small as argued in ref. [33]. The generation of D by stretching of vortex filaments and its destruction through viscous reduction of velocity gradients are modeled collectively as in ref. [34]. The buoyancy term in the D equation is approximated as

$$2\overline{\frac{\partial \rho'}{\partial x_j}\frac{\partial u_i'}{\partial x_j}} g_i = \frac{D}{k} C_{\varepsilon 3}\overline{\rho' u_i'} g_i. \tag{12}$$

When using the Boussinesq approximation, the RHS of equation (12) yields an expression commonly used in buoyant flows; see, for example, the review by Kumar [35]. The final forms of the modeled equations are,

$$\frac{\partial}{\partial t}(\bar{\rho}k) + \frac{\partial}{\partial x_j}(\bar{\rho}\bar{u}_j k) = \frac{\partial}{\partial x_j}\left[\left(\mu + \frac{\mu_t}{\sigma_k}\right)\frac{\partial k}{\partial x_j}\right] + P + G - \mu D - \overline{\rho' u_i'}\left(\frac{\partial \bar{u}_i}{\partial t} + \bar{u}_k\frac{\partial \bar{u}_i}{\partial x_k}\right) \tag{13}$$

†For incompressible turbulent flow, the D equation automatically implies an equation for ε. However, with ν variable, it is more convenient to solve the D equation first and then multiply the result by ν to obtain ε.

$$\frac{\partial}{\partial t}(\bar{\rho}D)+\frac{\partial}{\partial x_j}(\bar{\rho}\bar{u}_jD)$$
$$=\frac{\partial}{\partial x_j}\left[\left(\mu+\frac{\mu_t}{\sigma_\varepsilon}\right)\frac{\partial D}{\partial x_j}\right]+\frac{D}{k}(C_{\varepsilon1}P-C_{\varepsilon2}\mu D)$$
$$+\frac{D}{k}C_{\varepsilon3}G-\frac{D}{k}C_{\varepsilon3}\overline{\rho'u_i'}\left(\frac{\partial\bar{u}_i}{\partial t}+\bar{u}_k\frac{\partial\bar{u}_i}{\partial x_k}\right) \quad (14)$$

where: G and P are the buoyancy and shear production of turbulent kinetic energy, respectively (see Nomenclature); σ_k and σ_ε are the Prandtl numbers for k and ε which, like $C_{\varepsilon1}$, $C_{\varepsilon2}$ and $C_{\varepsilon3}$, are model constants.

In low turbulence flow, due, for example, to the presence of a wall or damping of the turbulent fluctuations by stable stratification, it is necessary to modify equation (14). The standard forced flow modification developed by Jones and Launder [18], subsequently used to predict turbulent free convection from a heated, vertical plate by Plumb and Kennedy [19] and Lin and Churchill [20], requires the inclusion of an extraneous term, $-2\nu(\partial k^{1/2}/\partial y)^2$, in the turbulent kinetic energy equation in order to be able to set $\varepsilon = 0$ at the wall. In this study such an empirical approach is avoided because ε is not zero at the wall and, although $-2\nu(\partial k^{1/2}/\partial y)^2$ is an adequate expression for ε in the near-wall region, it may be inappropriate in the bulk of the flow. Instead, ε at the wall is obtained by considering the balance of k in the viscous sublayer. In this region the k-equation is simply an expression equating viscous diffusion to dissipation of k

$$\frac{\partial}{\partial x_j}\left(\mu\frac{\partial k}{\partial x_j}\right)=\mu D. \quad (15)$$

The proof of equation (15) can be established by expanding fluctuating quantities in (13) in terms of Taylor series expansions in y, the distance perpendicular to the wall. Using a Taylor series expansion in y for $k^{1/2}$, it also follows that

$$k^{1/2}=\left(\frac{\partial k^{1/2}}{\partial y}\right)_w y+\cdots \quad (16)$$

with k at the wall taken as zero. The value of D at the wall is readily obtained by substituting the above result into equation (15)

$$D=2\left(\frac{\partial k^{1/2}}{\partial y}\right)_w^2. \quad (17)$$

There is ample evidence supporting the above arguments. First, $k \sim y^2$ as $y \to 0$ has been observed experimentally by Schubauer [36]; second, molecular diffusion of k balancing dissipation as $y \to 0$ has been observed to be a correct description of the turbulence energy budget by, for example, Laufer [37]; and third, $\varepsilon \to$ constant as $y \to 0$ is physically correct (see [38]).

Jones and Launder [18] also added an arbitrary term to the D-equation to obtain better agreement with experimental results of the turbulent kinetic energy in forced flow. Such a term is removed here because it cannot be justified in purely buoyant flow. This term was also dropped by Plumb and Kennedy [19] but was retained by Lin and Churchill [20].

In agreement with Jones and Launder [18] and Lam and Bremhorst [39], in this study C_μ and $C_{\varepsilon2}$ are made functions of Re_t, the turbulence Reynolds number, in order to account for low Reynolds number effects on the flow. The variation of C_μ is determined by requiring that the turbulence viscosity vary according to the Van Driest formulation in the near-wall region. The variation of $C_{\varepsilon2}$ is chosen so that the model will predict correctly the decay of isotropic grid turbulence for both high and low turbulence intensities. The modified parameters are,

$$C_\mu = C_{\mu_0}\exp\left[-2.5/(1+Re_t/50)\right] \quad (18a)$$

$$C_{\varepsilon2} = C_{\varepsilon2_0}[1-0.3\exp(-Re_t^2)]f_1(Re_t) \quad (18b)$$

where C_{μ_0} and $C_{\varepsilon2_0}$ are constants optimized for high Reynolds number flows. In equation (18b) $f_1 = 1-\exp(-Re_t^2)$ is a wall-damping factor applied between $y^+ = 0$ and 5 only. This is in order to comply with the requirements of a low Reynolds number formulation while simultaneously satisfying the condition that the third term on the RHS of equation (14) remain finite at the wall. Equation (18b) represents a compromise between the proposals in refs. [38] and [39].

In summary, the general Reynolds number form of the D-equation proposed here is equation (14) with C_μ, $C_{\varepsilon2}$ and μ_t given by (18a), (18b) and (10), respectively. Since there are no low Reynolds number modifications for the k equation, equation (13) is employed for both high and low Re_t flows. The boundary conditions for k and D at the wall, consistent with these equations, are

$$k_w = 0$$
$$D_w = 2\left(\frac{\partial k^{1/2}}{\partial y}\right)_w^2. \quad (19)$$

Finally, a relation for $\overline{T'^2}$ is also required in order to obtain $\overline{\rho'T'}$ from equation (7). The exact transport equation for $\overline{T'^2}$ is given in ref. [31]. Following Gibson and Launder [26], the assumption of a local equilibrium flow simplifies that equation to:

$$-2\bar{\rho}\overline{u_j'T'}\frac{\partial\bar{T}}{\partial x_j}=2\frac{\gamma}{C_p}\overline{\frac{\partial T'}{\partial x_j}\frac{\partial T'}{\partial x_j}}=\frac{1}{R}\frac{\nu D}{k}\bar{\rho}\overline{T'^2} \quad (20)$$

where the second equality, involving the model constant R, has been proposed by Launder [25]. Combining equations (7) and (20) yields the following relation for $\overline{\rho'T'}$:

$$\overline{\rho'T'}=2R\frac{k}{\nu D}\frac{\bar{\rho}}{\bar{T}}\overline{u_j'T'}\frac{\partial\bar{T}}{\partial x_j}. \quad (21)$$

Strictly speaking, equation (21) is only valid for high Re_t flows. It is used here since a satisfactory low Re_t approximation for the transport of $\overline{T'^2}$ does not yet exist. (Although we note that Plumb and Kennedy [19] have modeled the $\overline{T'^2}$-equation for flows where the

Boussinesq approximation applies, in a way similar to how Jones and Launder [18] modeled the k-equation. However, in addition to introducing an extra term in the $\overline{T'^2}$-equation, their model required the definition and optimization of three new constants.)

Equations (8)–(10), (13), (14) and (21) together with the mean transport equations (2)–(6) constitute an isotropic eddy viscosity model for calculating free (or mixed) convection turbulent flows.

2.3. *Algebraic stress model (ASM)*

Equations governing the transport of the Reynolds stresses $\overline{u_i'u_j'}$ and heat fluxes $\overline{u_i'T'}$ have been derived [31]. Simplified forms of the equations, obtained by neglecting third and higher order correlations involving ρ', $\partial u_i'/\partial x_i$ and the viscosity gradient terms, are the basis for the model used here. Apart from the production terms which are known exactly, the terms affecting the balances of $\overline{u_i'u_j'}$ and $\overline{u_i'T'}$ involve unknown correlations of fluctuating quantities. The modeling of these terms follows from the work of Launder and his colleagues [25–27] and is carefully outlined in ref. [31].

In modeling the pressure redistribution of $\overline{u_i'u_j'}$ and $\overline{u_i'T'}$, contributions due to fluctuating velocities and temperature (and their interactions), the mean strain (and its interactions with fluctuating velocities and temperature), buoyancy and wall damping effects are all considered. To render algebraic the complex system of differential equations for the turbulent fluxes, the assumption of a local equilibrium flow is invoked [40]. Although this assumption is incorrect for a low Reynolds number flow or in the proximity of a solid wall, KEM calculations show that, except in a viscous region very close to the wall, the turbulence Reynolds number is of the order of 10^2 to 10^3. Given this rapid tendency of the flow to acquire a high turbulence Reynolds number, the applicability (or not) to free convection of an ASM formulation premised on the local equilibrium assumption is perhaps better judged by the level of agreement found between measurements and predictions. Thus, *assuming* local equilibrium, the algebraic expressions resulting for $\overline{u_i'u_j'}$ and $\overline{u_i'T'}$ are,

$$0 = P_{ij} + G_{ij} + \pi_{ij} - \frac{2}{3}\mu D\left[(1-f_s)\delta_{ij} + \frac{3}{2}f_s\frac{\overline{u_i'u_j'}}{k}\right] \quad (22)$$

$$0 = -\bar{\rho}\overline{u_i'u_j'}\frac{\partial \bar{T}}{\partial x_j} + P_{iT} + \overline{\rho'T'}g_i + \pi_{iT}. \quad (23)$$

In the above expressions, $f_s = 1/(1+Re_v/10)$ is a low Reynolds number correction to the stress dissipation; π_{ij} and π_{iT} denote the pressure redistribution terms; and the following production terms due to shear and buoyant forces are defined

$$P_{ij} = -\bar{\rho}\left(\overline{u_j'u_k'}\frac{\partial \bar{u}_i}{\partial x_k} + \overline{u_i'u_k'}\frac{\partial \bar{u}_j}{\partial x_k}\right) \quad (24)$$

$$P_{iT} = -\bar{\rho}\overline{u_j'T'}\frac{\partial \bar{u}_i}{\partial x_j} \quad (25)$$

$$G_{ij} = \overline{\rho'u_i'}g_j + \overline{\rho'u_j'}g_i. \quad (26)$$

The π_{ij} and π_{iT} terms are complicated functions of k, D, $\overline{u_i'u_j'}$, $\overline{u_i'T'}$, P, G, P_{ij}, G_{ij} and P_{iT}. They involve the specification of various model constants and of a function, $f(l/y)$, to reduce the effect of the wall pressure corrections with increasing distance from the wall. The forms of these terms and of equations (22) and (23) for the case of flow along a heated, vertical, flat plate are given in detail in ref. [31].

Since k and D appear explicitly in the ASM formulation, they must also be calculated. Although k could be approximated from ASM calculations of $\overline{u_i'u_i'}$, in practice it is more convenient† to calculate k directly from its own transport equation and to determine two of the normal stresses via the ASM formulation. The third normal stress is evaluated as

$$\overline{u_j'^2} = 2k - \sum_{i\neq j}\overline{u_i'^2}. \quad (27)$$

As before, the turbulent diffusion of k and D by pressure fluctuations are neglected but the triple velocity correlations are modeled according to refs. [33] and [41]:

$$\frac{\partial}{\partial x_j}\left(-\bar{\rho}\overline{u_j'\frac{u_i'u_i'}{2}}\right) = \frac{\partial}{\partial x_j}\left(C_s'\frac{k}{\nu D}\bar{\rho}\overline{u_i'u_j'}\frac{\partial k}{\partial x_i}\right) \quad (28)$$

$$\frac{\partial}{\partial x_j}\left(-\bar{\rho}\overline{u_j'\frac{\partial u_i'}{\partial x_k}\frac{\partial u_i'}{\partial x_k}}\right) = \frac{\partial}{\partial x_j}\left(C_\varepsilon\frac{k}{\nu D}\bar{\rho}\overline{u_i'u_j'}\frac{\partial D}{\partial x_i}\right). \quad (29)$$

In flows that are two-dimensional in the mean, equations (20), (22) and (23) represent a system of six algebraic equations constaining $\overline{u'^2}$, $\overline{v'^2}$, $\overline{u'v'}$, $\overline{u'T'}$, $\overline{v'T'}$ and $\overline{T'^2}$ as unknowns. Together with the equations for k, D, $\overline{\rho'T'}$ (of the previous section) and the mean transport equations, the system is closed. In this study $\overline{w'^2}$ is evaluated by subtracting ASM-calculated values of $\overline{u'^2}$ and $\overline{v'^2}$ from values of k calculated from its own transport equation.

Values for the required model constants were taken from refs. [25], [28] and [30]. The values used are:

R	C_s'	C_ε	$C_{\varepsilon 1}$	$C_{\varepsilon 2_0}$	$C_{\varepsilon 3}$	Pr_t	C_{μ_0}	σ_k	σ_ε
0.8	0.24	0.15	1.44	1.92	1.44	0.9	0.09	1	1.3.

(30)

In addition, constants which appear in the model for the pressure redistribution terms must be specified. They are listed in ref. [31] where it is explained that three of the wall correction terms are nullified by the zero values of the constants. This state of affairs is due to a lack of appropriate experimental data from which to derive accurate values for these three constants. Although part of the inaccuracies in the present study may be due to the neglect of these terms, we have deliberately avoided

† It is also physically more realistic to determine k from a transport equation which retains the contributions of convection and diffusion to its overall balance.

attempting to obtain new estimates of *any* of the constants by seeking an improved agreement between measurements and predictions. Such an exercise must await the availability of an accurately determined and sufficiently extensive data base.

2.4. *Boundary conditions and related considerations*

The boundary conditions for the heated, vertical, flat plate flow are shown in Fig. 1. Since the governing equations solved here are fully elliptic, boundary conditions are needed along the solid wall and the three 'free' boundaries of the calculation domain.

There is no need to specify boundary conditions for the temperature fluctuations, $\overline{T'^2}$, since in both the KEM and ASM models this variable is evaluated algebraically. For the same reason, boundary conditions are not required in the ASM formulation for the turbulent stresses and heat fluxes.

(i) *The solid wall.* In forced convection, law-of-the-wall relations for velocity and temperature are frequently used to bridge the gap between the wall and the inertial region in the flow. This empirical practice saves considerable computing time and storage, but its extension to natural and mixed convection flows is questionable since, in general, it is not known what are the correct relations to apply. In principle, one could use power-law relations for velocity and temperature of the form derived by George and Capp [29] for the buoyant sublayer region of a heated, vertical, flat plate, but the constants in the relation for velocity are not known accurately, even at low $\Delta T/T_\infty$ (see Section 1.2). Thus it would seem that refining the calculation mesh and predicting the details of the flow *all the way to the wall* is the most assured alternative.

The present procedure requires specifying the value of the dissipation of turbulent kinetic energy at the wall. Using the low Reynolds number model of Jones and Launder [18], Plumb and Kennedy [19] and Lin and Churchill [20] carried their calculations all the way into the viscous sublayer while imposing a zero value for dissipation at the wall. As a result, their calculated 'dissipation' cannot be viewed as a true isotropic dissipation (see [42]). This difficulty can be overcome by evaluating the wall dissipation from the simplified form of the turbulent kinetic energy equation in the wall region: see equations (15)–(17). This condition for dissipation together with no slip impermeable wall conditions for velocity and a constant wall temperature

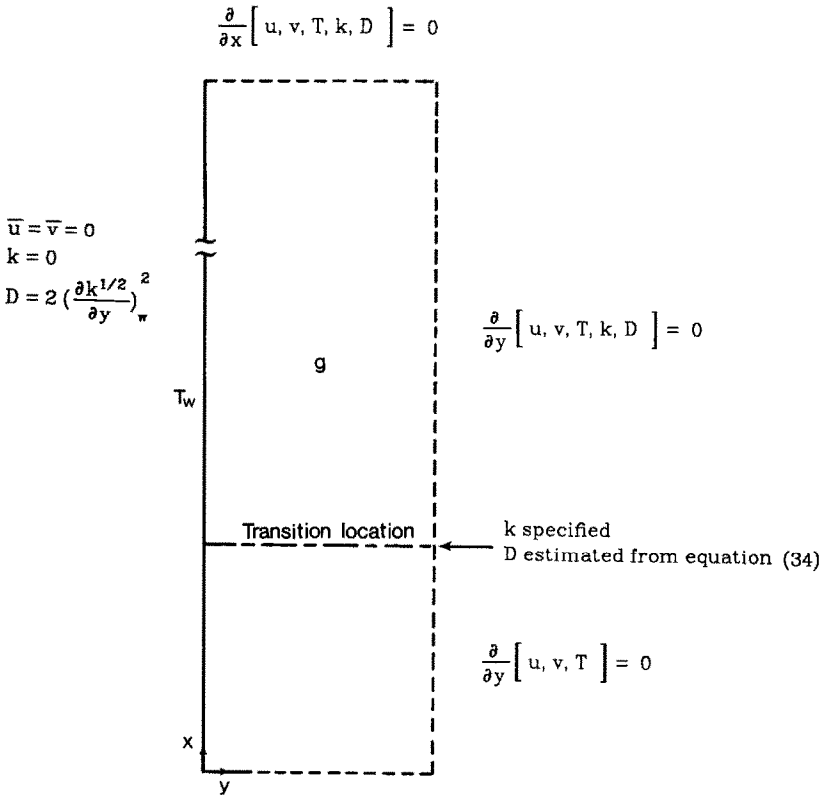

FIG. 1. Boundary conditions for heated, vertical, flat plate flow.

are summarized below:

$$\bar{u}_i = 0$$
$$\bar{T} = T_w$$
$$k = 0 \tag{31}$$
$$D = 2\left(\frac{\partial k^{1/2}}{\partial y}\right)_w^2.$$

An estimate of the thickness of the viscous sublayer region in free convection is needed to maintain the necessary grid refinement in the numerical calculations. This can be derived from the correlation obtained by George and Capp [29] who find

$$1.7 \approx \frac{y}{\eta_T} = y^+ \frac{y_\tau}{\eta_T} \tag{32}$$

where η_T is the inner region flow length scale. Using the LDV measurements in Cheesewright and Ierokipiotis [6] to estimate y_τ and η_T, y^+ is found to be approximately 4. During the course of calculation, the grid refinement is continuously checked against this criterion.

(ii) *The far field (free boundaries).* The free boundary conditions used are shown in Fig. 1. Velocity and temperature distributions along the upstream boundary were specified by imposing Ostrach's [43] laminar flow solution at a distance of 0.05 m from the leading edge of the plate. Zero normal gradient conditions were imposed for all varaibles on the downstream and side boundaries. The side boundary was placed at a distance from the plate equal to 3.5 times the boundary-layer thickness at the end of the place.

To initiate the turbulence calculations, a small amount of kinetic energy of turbulence (6×10^{-4} m^2 s^{-2}) was introduced at the experimentally observed transition points ($Gr_x = 2 \times 10^9$ for $\Delta T = 56$ K and $Gr_x = 1.5 \times 10^8$ for $\Delta T = 404$ K). The corresponding value of dissipation was then estimated from an approximate balance between shearing production and rate of dissipation. Thus, using the boundary-layer approximation,

$$\bar{\rho}\overline{u'v'}\frac{\partial \bar{u}}{\partial y} \approx \mu D \tag{33}$$

and equations (8) and (10) yield

$$D \approx \frac{C_\mu^{1/2}}{\mu}\bar{\rho}k\frac{\partial \bar{u}}{\partial y}. \tag{34}$$

Equations for the turbulence variables were solved numerically in the computational subdomain bounded by the transition plane, the downstream boundary, the wall and far-side free boundary. The remaining variables were computed throughout the entire computational domain.

2.5. *Numerical solution*

(i) *Methodology.* The REBUFFS code developed by LeQuere *et al.* [30] was extended to include the KEM and ASM turbulence model formulations described above. In REBUFFS, a control volume approach is adopted for obtaining finite-difference forms of the differential transport equations and their corresponding boundary conditions. This has been amply discussed in refs. [30] and [44]. Exactly the same approach is used to derive the additional difference equations required here for k, D and the turbulent fluxes. The final forms of the difference equations apply to variable physical property (temperature dependent) flows. Note that boundary-layer simplifications are not used in formulating the difference equations since these are needed in elliptic form for calculating recirculating flows in cavities (the subject of Part II of this work).

The methodology for performing the numerical calculations is described in ref. [30]. This involves an under-relaxed iteration sequence using an algorithm that is implicit in time. The extension to turbulent flow was achieved by introducing the calculation of k and D (followed by the calculation of the turbulent fluxes when using the ASM model) into the iteration sequence. No difficulties were experienced in obtaining steady-state results even when using very large time steps.

All calculations were performed using a hybrid upwind-central differencing scheme [44]. Special care was taken to establish the number and distribution of grid nodes required to generate essentially grid-independent results. A nonuniform grid consisting of 52 nodes in the streamwise direction, x, and 47 nodes in the cross-stream direction, y, was used. The cross-stream distribution of nodes was fixed by locating the first five nodes within the viscous sublayer ($y^+ < 4$) and expanding the rest of the grid from the wall using a factor of 6/5. The distribution of nodes in the streamwise direction was such that about nine nodes were contained in the laminar region, 17 nodes were in the transition region and 24 nodes were in the fully turbulent region. This partitioning of streamwise grid nodes depended on the value of $\Delta T = T_w - T_\infty$ since, for a fixed plate length L, the x-position for transition to turbulence was dictated by ΔT. Relative to calculations performed on a 52×36 grid, the 52×47 grid yielded a 0.4% change in total heat transfer and a 0.1% change in the maximum velocity.

The calculations were performed on the CDC 7600 machine at the Lawrence Berkeley Laboratory. KEM calculations using the finest grid required 265K octal words of computer storage and 0.5 s per iteration. About 500 iterations were necessary to obtain converged results. For the same grid, the convergence of ASM calculations was slower due to the additional iterations needed for solving the turbulent fluxes. The ASM calculations required 280K octal words of storage and 1.2 s per iteration. About 850 iterations were necessary to obtain converged results. Although substantial reductions in ASM computational times could be obtained by using converged KEM results as starting conditions, it was decided to conduct independent calculations in order to avoid any possible bias in the ASM results.

The convergence criterion was that the relative change of values of the variables between consecutive iterations at a critically located monitoring point should be less than 10^{-4} while simultaneously requiring that the respective sums of the absolute residual sources of mass, momentum, thermal energy, kinetic energy of turbulence and its rate of dissipation should all be less than 10^{-3}.

(ii) *Testing.* Various purely numerical aspects of the turbulent versions of the REBUFFS code were tested by calculating laminar free convection along a heated, vertical, flat plate. Excellent agreement was obtained with Ostrach's [43] analytical solution, both for the Nusselt number and the temperature and velocity profiles. The calculations were performed using a nonuniform grid of 27 nodes in the cross-stream direction and 20 nodes in the streamwise direction. The plate length was 0.5 m which, with $\Delta T = T_w - T_\infty = 349\text{–}293 = 56$ K, corresponds to a Grashof number of 1.1×10^9 and an overheat ratio of $\Delta T/T_\infty = 0.19$.

3. RESULTS AND DISCUSSION

3.1. *Preliminary considerations*

The production/destruction of turbulent kinetic energy due to buoyancy-driven flow along a heated, vertical, flat plate is $-\overline{\rho' u'} g$. Under the gradient assumption in the k–ε model this quantity is proportional to $-\partial \bar{T}/\partial x$ and, as a result, represents a destruction, albeit small, of turbulent kinetic energy. This contrasts with what should be expected from simple considerations of the term $-\overline{\rho' u'} g$, since one would anticipate a negative value of ρ' to correlate with a positive value of u' on average. Therefore, the term $-\overline{\rho' u'} g$ represents a *production* term, as opposed to a destruction term, in the balance of k. Because of the inconsistency arising as a result of assuming $\overline{\rho' u'} g \approx \partial \bar{T}/\partial x$, Mason and Seban [15] and Lin and Churchill [20] assumed that $\overline{\rho' u'} g$ is proportional to the *transverse* temperature gradient,

$$\overline{\rho' u'} g = \frac{1}{\bar{T}} \frac{\mu_t}{Pr_t} \frac{\partial \bar{T}}{\partial y} g. \tag{35}$$

No justification, other than the fact that the correct sense of contribution to k is now preserved, was given for this modified form of the gradient assumption. Nevertheless, these authors found that, at least for air, this contribution to k had a negligible effect on their numerical solutions and they therefore dropped the buoyancy term from the k-equation altogether. Plumb and Kennedy [19] assumed that $\overline{\rho' u'} \approx \sqrt{(\overline{T'^2} k)}$, but the constant of proportionality obtained by them is not universal. This is because the constant is of fixed sign and magnitude, and is specific to heated, vertical, flat plate flow. In fact, their assumption is not readily generalized to arbitrary stratified flows.

KEM test results from this study showed that whether $\overline{\rho' u'} \approx \partial \bar{T}/\partial y$ or zero the effect on calculations of heat transfer, mean temperature and velocity is negligible. However, the turbulent kinetic energy maximum is decreased by 7% if buoyancy is neglected. Estimates of the shearing production and buoyancy production/destruction of k (shown in Fig. 10) can be obtained from the measurements by Miyamoto *et al.* [8]. These results show that buoyancy production is relatively small, compared to shearing production, everywhere except in the vicinity of the velocity maximum, and towards the edge of the boundary layer where both contributions to k are small. The measurements also indicate that buoyancy production is negative, but small, in the viscous sublayer, which probably explains the insensitivity of calculated heat transfer results to the buoyant production of k.

As a result of the above, and in keeping with similar turbulence model approaches [15, 20], direct buoyant contributions to the balance of k and ε, the terms containing G in equations (13) and (14), have been neglected in the present vertical flat plate KEM calculations. This modeling difficulty does not arise in the ASM formulation since $\overline{\rho' u'}$ is computed from equation (6) using an algebraic expression for $\overline{u' T'}$.

While the turbulent Prandtl number, Pr_t, does not arise in the ASM formulation, it is a critical parameter in the KEM formulation for it controls the heat transfer. For example, calculations showed that changing Pr_t from 0.9 to 0.5 causes a reduction of 23% in the heat transfer. One can always refine Pr_t in accord with the experimental data as was done by, for example, Mason and Seban [15] and Plumb and Kennedy [19]. The former used a step function and the latter used a smooth function of y/δ (δ being the boundary-layer thickness). A constant value of 0.9 was used in the present KEM formulation as was used by Lin and Churchill [20]. A comparison between present KEM heat transfer results and the predictions of refs. [15] and [19] using variable turbulent Prandtl number formulations showed insignificant differences. Further discussion concerning the variation of Pr_t with distance from the wall is provided below.

The results predicted by the KEM and ASM formulations are presented in the following subsections. The results are compared to experimental data and earlier calculations wherever possible.

(i) *Heat transfer.* Heat transfer results are shown in Fig. 2 in the form of plots of Nu_x vs Gr_x. The correlation for low ΔT from Siebers *et al.* [10] represents the best fit to all low ΔT experimental measurements performed to date. The integral analysis results of Eckert and Jackson [11], Bayley [12], and the k–ε model calculations by Plumb and Kennedy [19] and Lin and Churchill [20] are in close agreement but fall above the best fit for low ΔT. Corresponding k–l model predictions by Mason and Seban [15] fall below the best fit for data at low ΔT and exactly on the best fit for the data at high ΔT. However, because their model is premised on the applicability of the Boussinesq approximation the latter agreement is not especially

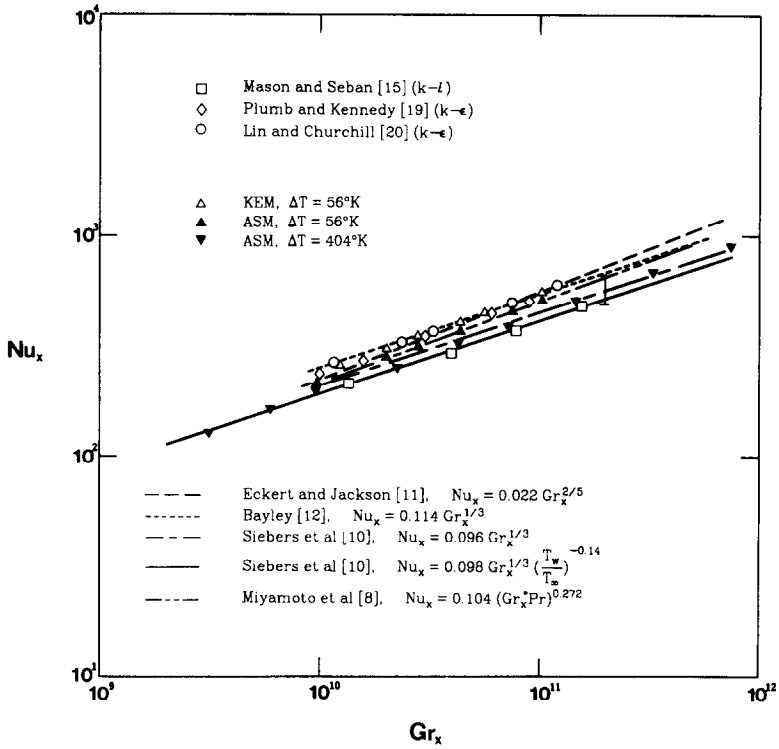

FIG. 2. Comparison between present KEM and ASM predictions of heated, vertical, flat plate, free convection flow and earlier calculations and measurements. Points refer to conditions actually predicted (KEM and ASM) or to interpolations from the numerical calculations of others. Dashed lines represent integral analysis results. Continuous lines are best fits to experimental data obtained by Siebers *et al.* [10]. Vertical bar denotes uncertainty bounds on data measured by Siebers *et al.* [10].

meaningful. Present ASM predictions for low ΔT show only a slight improvement over the KEM results. By contrast, at high ΔT the ASM predictions are in closer relative agreement with the high ΔT measurements of ref. [10]. Given the level of experimental uncertainty present in the measurements at both high and low ΔT, shown as a vertical bar in the figure, we must conclude that, in so far as the calculation of heat transfer from vertical flat plates is concerned, it would appear that the ASM is only marginally superior to the KEM.

Figure 3 provides a more detailed comparison between ASM-calculated Nu_x and the experimental correlations of ref. [10] as a function of Gr_x. The transition point to turbulent flow at high ΔT was taken as $Gr_x = 1.5 \times 10^8$, as observed in ref. [10]. However, numerical tests showed that the fully turbulent variation of Nu_x with Gr_x was ultimately independent of the choice of transition location. A similar observation has been made for low ΔT [15]. In the laminar flow regime the calculations are in very good agreement with the measurements and follow the $Gr_x^{1/4}$ dependence. Calculations in the turbulent flow regime follow closely the $Gr_x^{1/3}$ dependence and agree with the measurements to within experimental error.

(ii) *Mean velocity and temperature.* Predicted and measured streamwise velocity and temperature profiles are shown in Fig. 4 for low ΔT as a function of the nondimensional transverse coordinate, $\zeta = yNu_x/x$. The measurements of velocity correspond to separate experiments performed by Cheesewright [5] (using a hot wire) and by Cheesewright and Ierokipiotis [6] (using a laser–Doppler velocimeter). Both sets of data are shown here since the first measurements were the target for the predictions of Mason and Seban [15] and Plumb and Kennedy [19]. Subsequently it has been shown (see [6]) that the first measurements are in error and that the second are to be preferred. The latter have been the target for our study. The measurements for temperature correspond to constant wall temperature [5] and constant heat flux [8] boundary conditions, respectively. The close agreement between these two sets of data is attributed to having used the same characteristic length scale for correlating the results.

All the predictions of velocity are in reasonable agreement with the LDV measurements in ref. [6]. However, only the present KEM and ASM predictions are consistently good for *all* values of the transverse coordinate. Of these two, the ASM model yields a slightly better picture of the velocity component far-field behavior. Similar levels of agreement between measurements and predictions of temperature are obtained by Mason and Seban [15] and the present

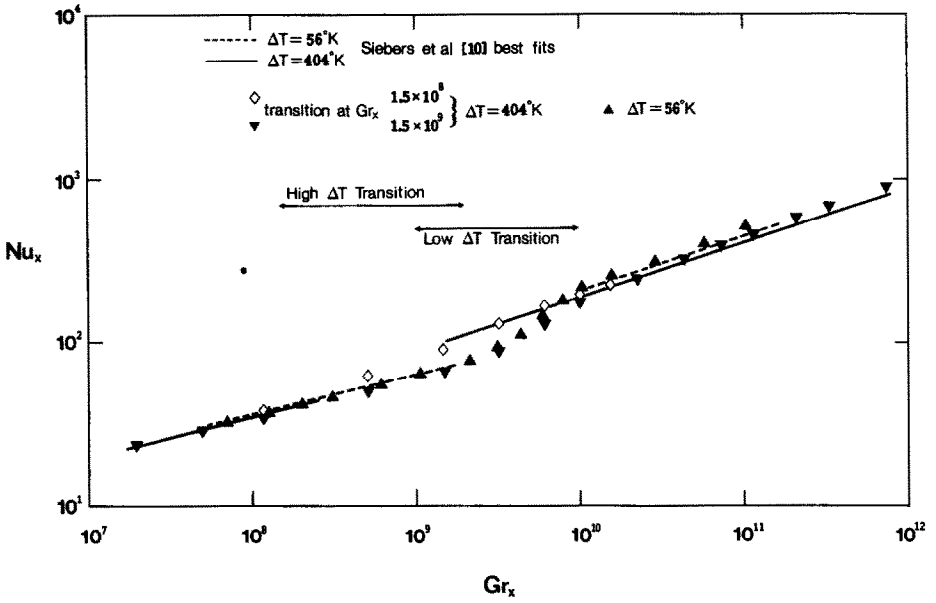

FIG. 3. Measured (best fit lines) and ASM-predicted (points) variation of Nu_x vs Gr_x for the free convection flow along a heated, vertical, flat plate. Gr_x values for triggering transition and transition ranges are indicated.

KEM and ASM model formulations. But as before, only the KEM and ASM results are consistently good for all values of ζ. The k–ε model predictions of Plumb and Kennedy [19] shows especially large discrepancies at intermediate values of ζ.

(iii) *Turbulence quantities.* Measured and ASM-calculated turbulent stresses and heat fluxes are shown in Figs. 5 and 6. The experimental velocity data were obtained using a laser–Doppler velocimeter. Temperature was measured using fine thermocouples. Although critical uncertainty analyses are not provided in refs. [6] or [8], Humphrey *et al.* [1] show that mean velocities in free convection flows can be determined fairly accurately using the LDV technique. However, the fluctuating components of motion are prone to large uncertainties. These are due, mainly, to inhomogeneous particle seeding and inhomogeneous refractive index effects or 'beam dancing'. Therefore, while we view the present comparisons as being of great importance for validating qualitative aspects of the ASM model, a quantitative optimization of the model is unjustified until definitive measurements of relevant turbulence quantities are available for this purpose.

The calculated streamwise component of turbulence intensity in Fig. 5, corresponding to low ΔT, shows an interesting variation. Between $\zeta = 0.5$ and 2 the rapid increase in $(\overline{u'^2})^{1/2}/\bar{u}_m$ is suddenly halted at a value of about 0.19. Since the calculated velocity maximum peaks at $\zeta = 1.8$ (Fig. 9) and $\overline{u'v'}$ goes through zero at about $\zeta = 1.5$ (Fig. 6), for low ΔT the shearing production of $\overline{u'^2}$, equation (24), is minimized between $\zeta = 1.5$ and 1.8 approximately. (In point of fact this is a region of small 'negative' production.) Similarly, the buoyancy production of this component [equation (26)] is also small in this region. This can be shown by substitution of equation (6) in (26) and noting from Fig. 6 that the calculated $\overline{u'T'}$, for low ΔT, goes through zero at about $\zeta = 1.4$. Although there are discrepancies between the calculations and measurements for $(\overline{u'^2})^{1/2}/\bar{u}_m$, the experimental data also show a temporary halting in the growth of this component when it reaches a value of about 0.21.

It seems reasonable to assume that, with the shear and buoyancy production of $\overline{u'^2}$ suppressed, pressure redistribution of energy from this component to $\overline{v'^2}$ and $\overline{w'^2}$ should work to further reduce the value of $\overline{u'^2}$. The anisotropic influence of wall damping should be expected to favor energy transfer to $\overline{w'^2}$ over $\overline{v'^2}$ and, in fact, Fig. 5 shows that $\overline{w'^2}$ is considerably larger than $\overline{v'^2}$ in the near-wall region of the flow. Further away from the wall, shearing and buoyant production once again increase the level of $\overline{u'^2}$. Reduced wall-damping of $\overline{v'^2}$ allows this component to increase through pressure-redistribution of energy. By contrast, the $\overline{w'^2}$ component decreases markedly in the outer flow region for which there is no immediately obvious explanation. However, we note that this component is found from $\overline{w'^2} = 2k-(\overline{u'^2}+\overline{v'^2})$, where $\overline{u'^2}$ and $\overline{v'^2}$ are calculated from algebraic relations obtained by neglecting convection and diffusion in the respective stress transport equations. The profiles in Fig. 10 (discussed below) show that convection and turbulent diffusion significantly affect the balance of k. In particular, turbulent diffusion works to transport k from the outer flow to the near wall region. As a result, the

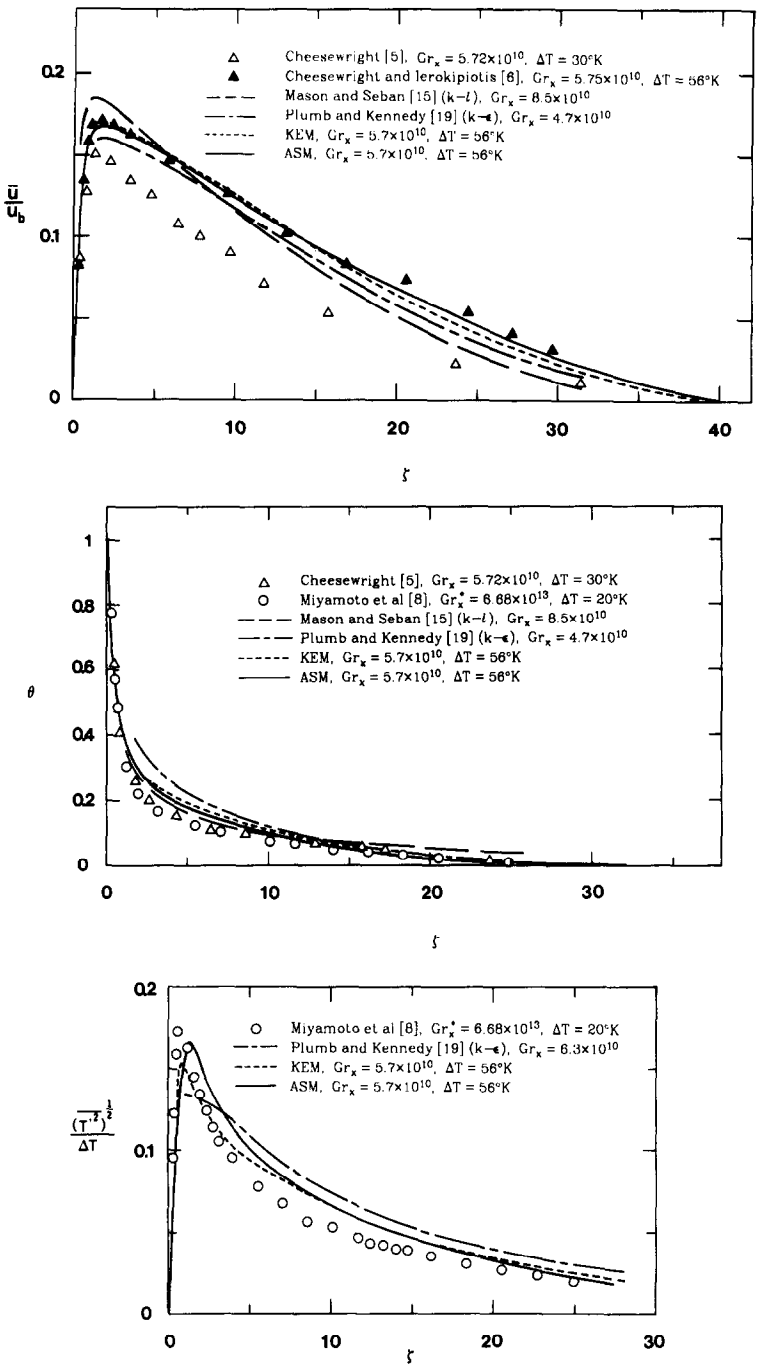

FIG. 4. Measured (points) and predicted (lines) of streamwise velocity, temperature and temperature fluctuation profiles in the turbulent region of free convection flow along a heated, vertical, flat plate at low ΔT.

ASM-calculated values of $\overline{u'^2}$ and $\overline{v'^2}$ are somewhat overestimated while values for $\overline{w'^2}$ are underestimated in the outer flow region. Assuming that $\overline{v'^2}$ has been calculated correctly (see Fig. 5) the amount by which the ASM-calculated value of $\overline{w'^2}$ should be adjusted is approximately the difference between the measured and calculated values of $\overline{u'^2}$. Thus, the near-wall peak value of $\overline{w'^2}$ would be slightly reduced while the outer-flow region values would be substantially increased.

Predictions of the turbulent shear stress, $\overline{u'v'}$, and of the heat fluxes, $\overline{u'T'}$ and $\overline{v'T'}$, are shown as appropriately normalized quantities in Fig. 6 for $\Delta T = 56$ K and $\Delta T = 404$ K. The results are in good qualitative agreement with the measurements. In particular, the experimentally observed regions of negative $\overline{u'v'}$ and $\overline{u'T'}$ are resolved numerically, and it is

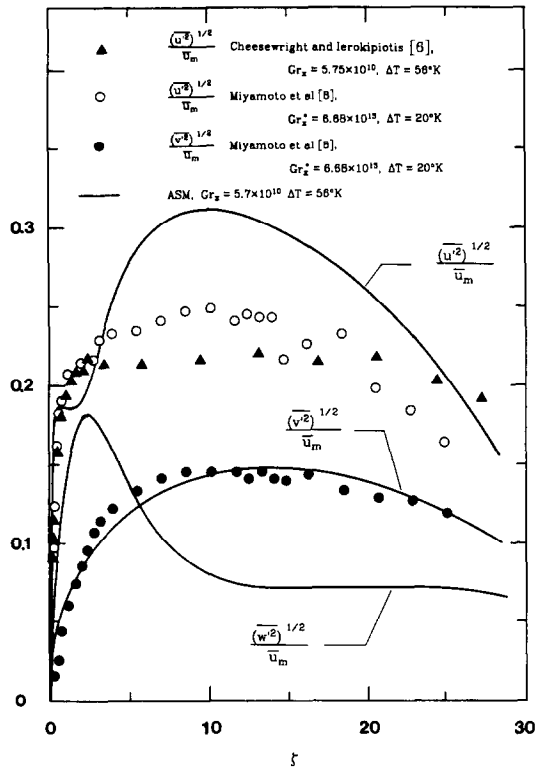

FIG. 5. Measured (points) and predicted (lines) normal components of turbulent stress in free convection flow along a heated, vertical, flat plate at low ΔT.

clear from the calculations that the positions of zero shear stress and zero transverse gradient of the streamwise velocity component do not coincide. The rather large absolute differences between profiles computed for $\Delta T = 56$ K and 404 K are due to the temperature-dependent factors used for normalization. It is clear from the plots that the *shape* of the profiles for the turbulent fluxes are essentially independent of variations in ΔT. The systematic overprediction of the turbulent fluxes of momentum and heat in the near-wall region is partly due to the neglect of convection and diffusion in the models for these variables. It is interesting to note that because $\overline{u'T'} < 0$ very near the wall ($\zeta < 1.4$ for $\Delta T = 56$ K), equation (6) gives $\overline{\rho' u'} > 0$. As a consequence, term G in equation (13) for k is negative, which implies a *damping* of turbulent kinetic energy in this region *due to buoyant effects*; see also Fig. 10 discussed further below.

Measurements and calculations of the temperature fluctuations, $\overline{T'^2}$, are provided in Fig. 4. Of the three calculations shown, the ASM prediction comes nearest to matching the magnitude of $\overline{T'^2}$ near the wall while the KEM does a slightly better job of predicting its location. These near-wall differences are attributed to the way $\overline{u_j' T'}$ is evaluated in each case. Both models overpredict the far field values of $\overline{T'^2}$. Neither of the near-wall features (magnitude/location) is well predicted by ref. [19]. Assuming that the measurements are correct, we can only conclude that the present model for $\overline{T'^2}$, equation (20), is superior.

From the ASM calculations it is possible to obtain the quantity

$$Pr_t = [(\overline{u'v'})/(\overline{v'T'})]\frac{\partial \bar{T}/\partial y}{\partial \bar{u}/\partial y} = f(\zeta) \qquad (36)$$

for both high and low ΔT. The results are shown in Fig. 7 together with estimates of Pr_t obtained from the free convection data of Miyamoto *et al.* [8]. Unfortunately, the experiments were not performed for identical conditions. Thus the bars in the figure compound variations *between* experiments with uncertainties *within* experiments. Notwithstanding, the trend in the data supports the calculated variation of Pr_t with distance from the wall. The calculated distributions peak between the locations of maximum shear stress and maximum velocity and show a relatively pronounced dependence on temperature. Noting that a value of $\zeta = 6$ corresponds to a $y^+ = 115$, approximately, present results show Pr_t *decreasing* between $y^+ \sim 115$ and the wall. This contrasts with the variation known to arise in forced convection air flows (see, for example, [45]) where Pr_t *increases* from about 1 to 2 as y^+ decreases from 60 to 10. It is seen from Fig. 7 that a constant value of $Pr_t = 0.9$ for the KEM calculations is a reasonable choice.

(iv) *Near-wall results.* The near-wall results need further discussion since this is where the resultant flow and heat transfer are controlled. Attempts to plot velocity distributions in terms of wall variables (u^+ vs y^+) did not yield meaningful results. Although the profiles showed regions in which the velocity distributions could be approximated by logarithmic functions, the functions required different values of the Von Karman constant depending on the overheat ratio and Grashof number.

A comparison using a 1/3 power law is shown in Fig. 8. Due to the large ΔT range considered numerically, a film temperature, $T_f = (T_w + T_\infty)/2$, has been used to evaluate physical properties. The measurements are reasonably well correlated by the 1/3 power law in the buoyant sublayer, but with a displacement constant and slope different from that proposed in [29]. (In all fairness, it should be noted that the data available to George and Capp [29] for determining the power law constants was scanty and subject to unquantified uncertainty.) The predictions show that the dependence of the near-wall velocity distribution on temperature is only moderate. The forms of the calculated correlations are:

$$\frac{\bar{u}}{u_T} = 16.5\left(\frac{y}{\eta_T}\right)^{1/3} - 9.9 \quad (\Delta T = 56 \text{ K}) \qquad (37a)$$

and

$$\frac{\bar{u}}{u_{T_f}} = 16.5\left(\frac{y}{\eta_{T_f}}\right)^{1/3} - 11.3 \quad (\Delta T = 404 \text{ K}). \qquad (37b)$$

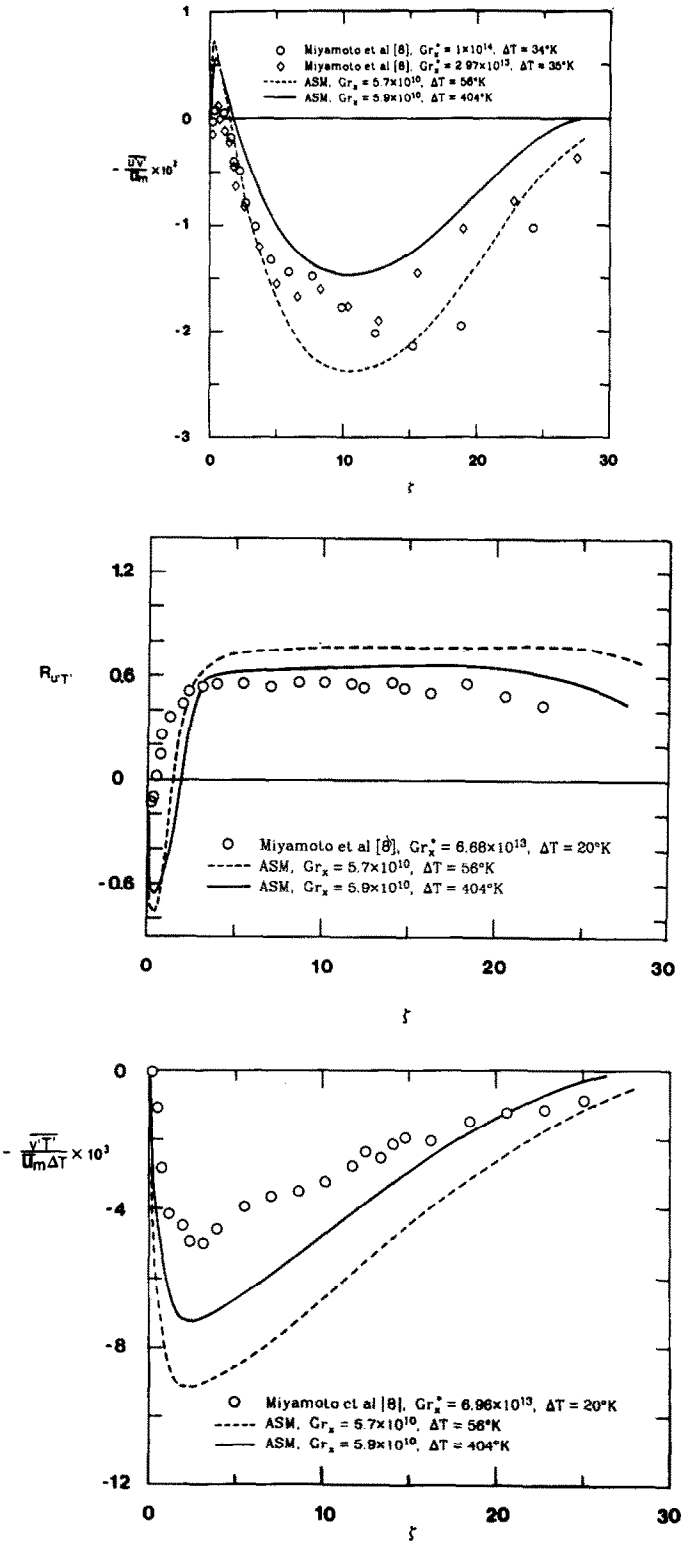

FIG. 6. Measured (points) and predicted (lines) values of turbulent shear stress and heat fluxes in free convection flow along a heated, vertical, flat plate.

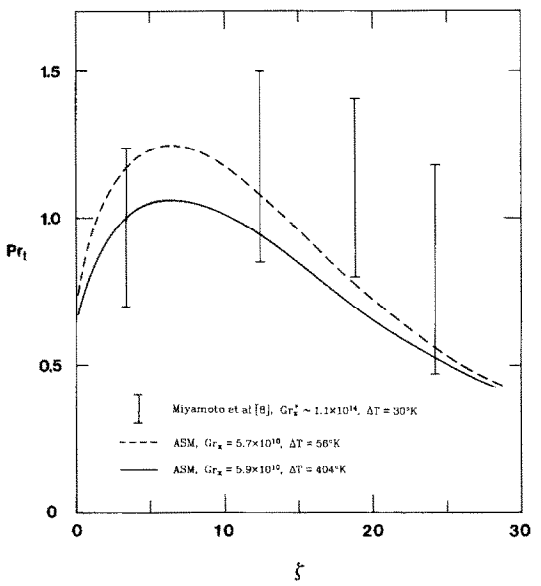

FIG. 7. Variation of Pr_t with distance from the wall for free convection along a heated, vertical, flat plate.

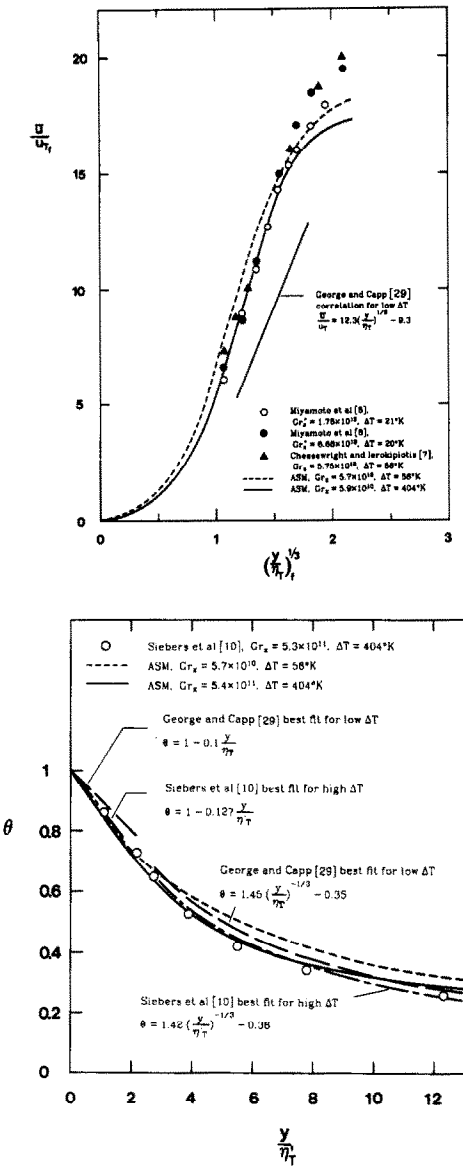

FIG. 8. Measured and ASM-predicted near-wall variations of streamwise velocity and temperature for free convection along a heated, vertical, flat plate. Velocity coordinates suggested by George and Capp [29]. Temperature abscissa coordinate suggested by Siebers *et al.* [10].

An attempt to obtain a single correlation valid for both high and low ΔT using $\eta_T' = \eta_T(\gamma_w/\gamma_\infty)(T_w/T_\infty)^{0.14}$, as suggested for temperature in ref. [10], proved unsuccessful. Experimental data in the linear region, $(y/\eta_T)^{1/3} \leqslant 1.2$ according to [29], are lacking and it is not possible to judge quantitatively the accuracy of the model calculations.

Near-wall measured and calculated temperature profiles are compared in Fig. 8 with the analytical formulations derived in ref. [29] for the viscous and buoyant sublayer regions. Agreement between the measurements of ref. [10] and present calculations is very good, especially at $\Delta T = 404$ K. While the temperature variation through the buoyant sublayer is well approximated by the expression derived in ref. [29], that obtained for the viscous region departs significantly from both the measurements and calculations. The temperature correlations calculated numerically are:

$$\theta = 1.35\left(\frac{y}{\eta_T}\right)^{-1/3} - 0.27 \quad (\Delta T = 56\ \text{K}) \quad (38a)$$

and

$$\theta = 1.28\left(\frac{y}{\eta_T'}\right)^{-1/3} - 0.28 \quad (\Delta T = 404\ \text{K}). \quad (38b)$$

These results show clearly that it is inappropriate to use logarithmic relations, derived from considerations of forced convection flow, as boundary conditions in free convection flow for patching a wall with the fully turbulent region. Instead, as suggested in ref. [29], a 1/3 power law appears to provide a good representation of both velocity and temperature variations in the buoyant sublayer region in free convection flow.

(v) *Overheat effects.* Calculations were performed to establish the influence of varying $\Delta T/T_\infty$ on turbulent free convection along a heated, vertical, flat plate. Some of the results obtained are shown in Fig. 9.

The mean velocity and temperature profiles reveal a strong dependence on ΔT in the near-wall region of the flow (between the wall and the velocity maximum). By contrast, the outer region shows a stronger dependence on Gr_x than on ΔT. Given that 60% of the temperature drop takes place between the wall and the velocity maximum, the latter result is not too surprising. As ΔT increases, the characteristic thermal spreading distance of the boundary layer increases and, since the Prandtl

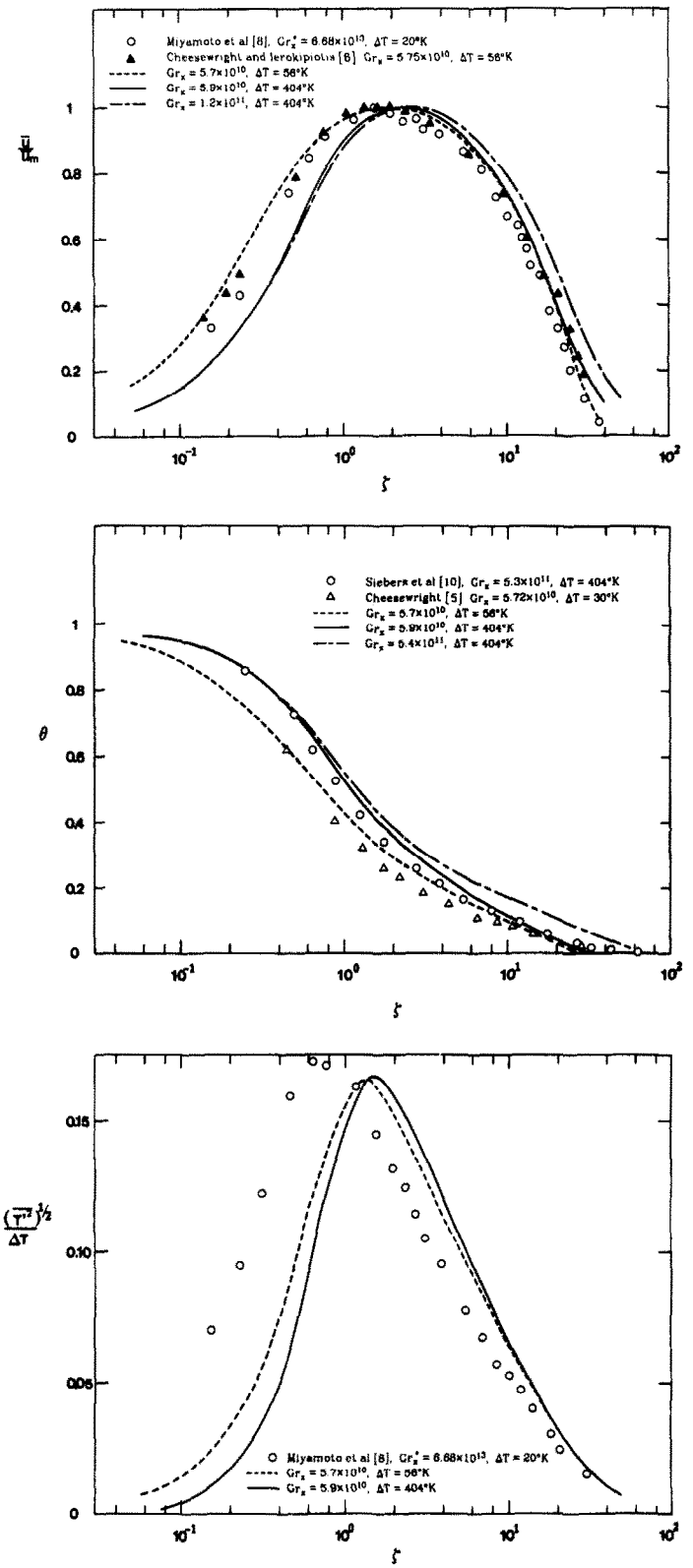

FIG. 9. Measurements and ASM predictions of streamwise velocity, temperature and temperature fluctuations for free convection along a heated, vertical, flat plate for two values of ΔT.

number in this temperature range is constant, the corresponding viscous spreading length must also increase. The strong reduction in $\bar{u}/\bar{u}_m$ with increasing ΔT near the wall is attributed to the temperature dependence of viscosity which, for air, increases as $\sqrt{T}$. This has the effect of increasing viscous forces relative to buoyant forces in the near-wall region and slows down the flow. The same variations with ΔT have been observed experimentally and predicted theoretically in the laminar flow study of Cairnie and Harrison [7].

Calculations of the turbulent kinetic energy and the normal stress components, available in ref. [31], show that increasing temperature has the effect of decreasing the relative turbulence intensity of the three normal stress components; although the $\overline{u'^2}$ component shows a small increase in the near-wall region.

A comparison between measured and predicted values of $\overline{T'^2}$ shows good qualitative agreement. Near-wall values of $\overline{T'^2}$ are unpredicted while the outer flow values are overpredicted. This is partly attributed to the neglect of convection and diffusion in the model for $\overline{T'^2}$. As for k, turbulent diffusion is expected to transport $\overline{T'^2}$ from the outer to the inner region of the flow, but this has not been accounted for in the model.

The turbulent kinetic energy budget was calculated for low and high ΔT. The low ΔT results are shown in Fig. 10. The physical contributions to the balance of k are identified in the figure. At high ΔT, the small region of negative shearing production (located around the velocity maximum) almost disappears. By contrast, the region of viscous diffusion extends further from the wall, although the relative magnitude of this effect is smaller at high ΔT. Aside from these differences, the profiles for each term in the budget show similar variations for both low and high ΔT.

Everywhere, dissipation and convection represent sinks in the balance of k. Near the wall the loss of k through dissipation becomes very large where it is balanced almost exclusively by shearing production. Shearing production becomes very small near the maximum velocity location and dissipation is now balanced essentially by an influx of k through turbulent diffusion from the near-wall and outer-flow regions. In the far field, turbulent diffusion also works to transport k away from the wall. In this region turbulent diffusion and shearing production are essentially balanced by dissipation and convection.

Except for a region bounded roughly by $y/\delta_u = 0.075$ and 0.3, buoyancy production is always less than shearing production. Between $y/\delta_u = 0$ and 0.075 the buoyancy term is negative and works to dampen turbulent fluctuations in the flow. Between $y/\delta_u = 0.075$ and 0.3 the dissipation of k is approximately balanced by the combined effects of buoyancy production, shear production and turbulent diffusion.

4. CONCLUSIONS

Two low Reynolds number turbulence model formulations have been developed for predicting wall-bounded, variable property, free convection flows. The KEM model relates turbulent fluxes to eddy viscosities via a generalized Boussinesq hypothesis. The ASM model calculates the turbulent fluxes from algebraic expressions derived from simplified forms of transport equations for the fluxes. For this, the main assumption is that of an equilibrium turbulent flow. Both models include wall-damping effects on turbulent transport. For the KEM model this involves introducing a turbulence Reynolds number dependence along

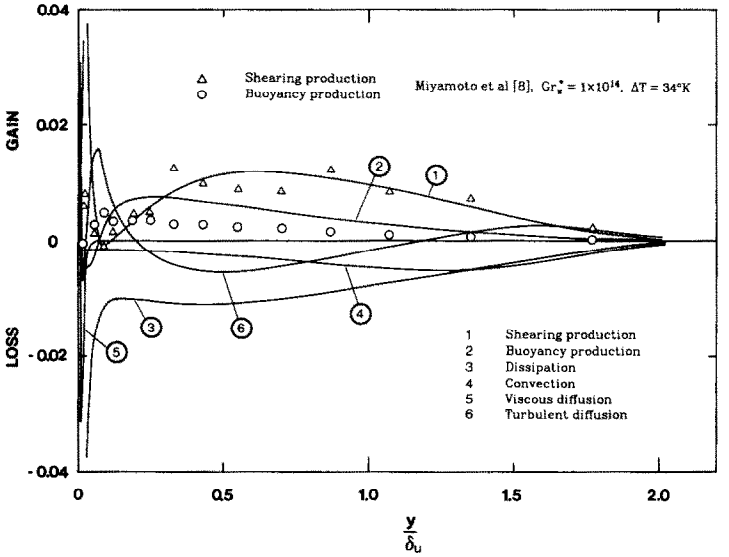

FIG. 10. Energy budget, normalized by $(\rho_\infty \bar{u}_m^3/\delta_u)$, for low ΔT (56 K) and $Gr_x = 5.6 \times 10^{10}$.

the lines of a Van Driest formulation for turbulent viscosity. In addition, the ASM model includes pressure redistribution and wall-damping effects on the transport of the turbulent fluxes.

Standard closure practices have been extended and improved to accommodate the needs of the present flow. These include retaining buoyancy production terms in the turbulent kinetic energy and the turbulent flux equations in the ASM formulation. The use of additional auxiliary relations derived from the equation of state, valid for air, facilitate the calculations of high temperature flows which do not follow the Boussinesq approximation. It has not been necessary to introduce new model constants into the model formulations. Values for the constants used have been taken from the literature. Further optimization of the constants must await the availability of more accurate and extensive experimental data relating to turbulence quantities.

Both models predict well the heat transfer and the mean flow characteristics of a heated, vertical, flat plate with the ASM model performing slightly better. In addition, the ASM model yields predictions of the anisotropic turbulence characteristics which are in good qualitative agreement with available experimental results. The discrepancies observed are possibly due, at least in part, to the assumption of an equilibrium flow, but the lack of an experimental uncertainty analysis makes this difficult to quantify. Near-wall computations support a $y^{1/3}$ dependence for velocity and a $y^{-1/3}$ dependence for temperature in the buoyant sublayer. Values of the power law constants for velocity and temperature (derived numerically) are presented here for the first time.

Predictions of the budget for turbulent kinetic energy show that in the outer-flow region all terms in the balance are of comparable magnitude. In the neighborhood of the velocity maximum, dissipation is balanced primarily by turbulent diffusion. Between this maximum and the wall, the buoyancy production term is negative and works to dampen turbulent fluctuations. In this region dissipation is balanced primarily by shearing production.

Acknowledgements—Funding for this study was provided by Sandia National Laboratories, Livermore, through Contract No. 20-1012. We gratefully acknowledge this support and the keen interest shown in the work by our colleagues at Sandia. The authors are indebted to Professor B. E. Launder at UMIST for useful discussions during the early stages of this work and to Professor F. S. Sherman at UCB who provided many useful comments and constant encouragmeent throughout the entire investigation.

REFERENCES

1. J. A. C. Humphrey, F. S. Sherman and K. Chen, Experimental study of free and mixed convective flow of air in a heated cavity, Contractor Report No. SAND84-8192, Sandia National Laboratories, Livermore, CA (1985).
2. C. Y. Warner and V. S. Arpaci, An experiential investigation of turbulent natural convection in air at low pressure along a vertical heated flat plate, *Int. J. Heat Mass Transfer* **11**, 397–406 (1968).
3. G. S. H. Lock and F. J. deB. Trotter, Observations on the structure of a turbulent free convection boundary layer, *Int. J. Heat Mass Transfer* **11**, 1225–1232 (1968).
4. R. J. Goldstein and E. R. G. Eckert, The steady and transition free convection boundary layer on a uniformly heated vertical plate, *Int. J. Heat Mass Transfer* **1**, 208–218 (1960).
5. R. Cheesewright, Turbulent natural convection from a vertical plane surface, *J. Heat Transfer* **90**, 1–8 (1968).
6. R. Cheesewright and E. Ierokipiotis, Velocity measurements in a turbulent natural convection boundary layer, *Proc. 7th Int. Heat Transfer Conference*, Vol. 2, pp. 305–309, Munich, F.R.G. (1982).
7. L. R. Cairnie and A. J. Harrison, Natural convection adjacent to a vertical isothermal hot plate with a high surface-to-ambient temperature difference, *Int. J. Heat Mass Transfer* **25**, 925–934 (1982).
8. M. Miyamoto, H. Kajino, J. Kurima and I. Takanami, Development of turbulence characteristics in a vertical free convection boundary layer, *Proc. 7th Int. Heat Transfer Conference*, Vol. 2, pp. 323–328, Munich, F.R.G. (1982).
9. R. Cheesewright and K. S. Doan, Space–time correlation measurements in a turbulent natural convection boundary layer, *Int. J. Heat Mass Transfer* **21**, 911–921 (1978).
10. D. L. Siebers, R. J. Moffat and R. G. Schwind, Experimental, variable properties natural convection from a large, vertical, flat surface, *J. Heat Transfer* **107**, 124–132 (1985).
11. E. R. G. Eckert and T. W. Jackson, Analysis of turbulent free convection boundary layer on a flat plate, N.A.C.A. Technical Report 1015 (1951).
12. F. J. Bayley, An analysis of turbulent free-convection heat transfer, *Proc. Inst. mech. Engrs* **169**, 361–370 (1955).
13. P. H. Oosthuizen, Heat transfer by turbulent free-convection from a vertical plate, *S. Afr. mech. Engng* **16**, 260–264 (1967).
14. H. Kato, N. Nishiwaki and M. Hirata, On the turbulent heat transfer by free convection from a vertical plate, *Int. J. Heat Mass Transfer* **11**, 1117–1125, (1968).
15. H. B. Mason and R. A. Seban, Numerical predictions for turbulent free convection from vertical surfaces, *Int. J. Heat and Mass Transfer* **17**, 1329–1336 (1974).
16. T. Cebeci and A. Khattab, Prediction of turbulent-free-convective-heat transfer from a vertical flat plate, *J. Heat Transfer* **97C**, 469–471 (1975).
17. D. L. Siebers, Natural convection heat transfer from an external receiver, SAND78-8276, Sandia National Laboratories, Livermore, CA (1978).
18. W. P. Jones and B. E. Launder, The prediction of laminarization with a two-equation model of turbulence, *Int. J. Heat Mass Transfer* **15**, 301–314 (1972).
19. O. A. Plumb and L. A. Kennedy, Application of a k–ε turbulence model to natural convection from a vertical isothermal surface, *J. Heat Transfer* **99**, 79–85 (1977).
20. S. J. Lin and S. W. Churchill, Turbulent free convection from a vertical isothermal plate, *Numer. Heat Transfer* **1**, 129–145 (1978).
21. B. E. Launder, Heat and mass transport. In *Turbulence* (edited by P. Bradshaw), *Topics in Applied Physics*, Vol. 12, pp. 231–287. Springer, Berlin (1978).
22. M. Hirata, H. Tanaka, H. Kawamura and N. Kasagi, Heat transfer in turbulent flows, *Proc. 7th Int. Heat Transfer Conference*, Vol. 1, pp. 31–57, Munich, F.R.G. (1982).
23. M. S. Hossain and W. Rodi, A turbulence model for buoyant flows and its application to vertical buoyant jets. In *Turbulent Buoyant Jets and Plumes* (edited by W. Rodi). Pergamon Press, Oxford (1982).
24. D. D. Gray and A. Giorgini, The validity of the Boussinesq

approximation for liquids and gases, *Int. J. Heat Mass Transfer* **19,** 545–551 (1976).
25. B. E. Launder, On the effects of a gravitational field on the turbulent transport of heat and momentum, *J. Fluid Mech.* **67,** 569–581 (1975).
26. M. M. Gibson and B. E. Launder, Ground effects on pressure fluctuations in the atmospheric boundary layer, *J. Fluid Mech.* **86,** 491–511 (1978).
27. M. M. Gibson and B. E. Launder, On the calculation of horizontal, turbulent, free shear flows under gravitational influence, *J. Heat Transfer* **98C,** 81–87 (1976).
28. M. Ljuboja and W. Rodi, Prediction of horizontal and vertical turbulent buoyant wall jets, *J. Heat Transfer* **103,** 343–349 (1981).
29. W. K. George and S. P. Capp, A theory for natural convection turbulent boundary layers next to heated vertical surfaces, *Int. J. Heat and Mass Transfer* **22,** 813–826 (1979).
30. P. LeQuere, J. A. C. Humphrey and F. S. Sherman, Numerical calculation of thermally driven two-dimensional unsteady laminar flow in cavities of rectangular cross section, *Numer. Heat Transfer* **4,** 249–283 (1981).
31. J. A. C. Humphrey, F. S. Sherman and W. M. To, Numerical simulation of buoyant turbulent flow, Contractor Report No. SAND85-8180, Sandia National Laboratories, Livermore, CA (1985).
32. B. E. Launder and D. B. Spalding, The numerical computation of turbulent flows, *Comput. Meth. appl. Mech. Engng* **3,** 269–289 (1974).
33. K. Hanjalic and B. E. Launder, A Reynolds stress model of turbulence and its applications to thin shear layers, *J. Fluid Mech.* **52,** 609–638 (1972).
34. K. Hanjalic and B. E. Launder, Contributions towards a Reynolds-stress closure for low-Reynolds-number turbulence, *J. Fluid Mech.* **74,** 593–610 (1976).
35. S. Kumar, Mathematical modelling of natural convection in fire—a state of the art review of the field modelling of variable density turbulent flow, *Fire Mater.* **7,** 1–24 (1983).
36. G. B. Schubauer, Turbulent processes as observed in boundary layer and pipes, *J. appl. Phys.* **25,** 188–196 (1954).
37. J. Laufer, The structure of turbulence in fully developed pipe flow, N.A.C.A. report No. 1174 (1954).
38. W. C. Reynolds, Computation of turbulent flows, *A. Rev. Fluid Mech.* **8,** 183–208 (1976).
39. C. K. G. Lam and K. Bremhorst, A modified form of the k–ε model for predicting wall turbulence, *J. Fluids engng* **13,** 456–460 (1981).
40. W. Rodi, A new algebraic relation for calculating the Reynolds stresses, *Mech. Fluid, Z. angew. Math. Mech.* **56,** T219 (1976).
41. B. J. Daly and F. H. Harlow, Transport equations of turbulence, *Phys. Fluids* **13,** 2634–2649 (1970).
42. K. Y. Chien, Predictions of channel and boundary-layer flows with a low-Reynolds-number turbulence model, *AIAA Jl* **20,** 33–38 (1982).
43. S. Ostrach, An analysis of laminar free convection flow and heat transfer about a flat plate paralell to the direction of the generating body force, NACA Technical Note 2635 (1952).
44. S. V. Patankar, *Numerical Heat Transfer and Fluid Flow.* Hemisphere/McGraw-Hill, New York (1980).
45. W. M. Kays and M. C. Crawford, *Convective Heat and Mass Transfer.* McGraw-Hill, New York (1980).

SIMULATION NUMERIQUE D'UN ECOULEMENT TURBULENT LIBRE. I—CONVECTION NATURELLE LE LONG D'UNE PLAQUE VERTICALE CHAUDE

Résumé—On développe deux modèles pour prédire la convection naturelle turbulente à faible nombre de Reynolds. Ces modèles s'appliquent aussi à la convection mixte. Le premier, du type k–ε, est basé sur la notion de diffusivités turbulentes de la quantité de mouvement et de la chaleur. Le second, un modèle algébrique de contrainte, est basé sur des approximations dérivées de flux turbulents anisotropes par une troncature convenable de leurs équations de conservation. Les deux formulations s'appliquent aux écoulements à propriétés variables avec des rapports élevés $\Delta T/T_\infty$. Il n'y a pas d'adaptation des valeurs des constantes pour obtenir un accord entre les mesures et les prévisions. Les formes elliptiques des équations de transport, avec leurs conditions aux limites appropriées, sont résolues numériquement pour deux cas bidimensionnels. Le premier correspond à la convection naturelle le long d'une plaque verticale chauffée et il fait l'objet de cet article. Le second correspond à la convection dans une cavité chauffée, de section rectangulaire arbitraires et d'orientation variable, étudié dans une seconde partie. Pour le premier cas, une comparaison entre les mesures et les prédictions montre que les deux modèles donnent des résultats précis pour l'écoulement moyen et le transfert thermique. Les distributions pariétales de vitesse et de température révèlent la loi puissance 1/3 de George et Capp [*Int. J. Heat Mass Transfer* **22,** 813–828 (1979)] et confirmée pour la température par Siebers *et al.* [*J. Heat Transfer* **167,** 124–134 (1985)]. Les valeurs des constantes des lois puissances pour la vitesse et la température sont obtenues numériquement pour $\Delta T/T_\infty$ faible et grand. Les contraintes de Reynolds et les distributions de flux de chaleur sont en bon accord qualitatif avec les mesures de Miyamoto et alii [*Proc. 7th Int. Heat Transfer Conference*, Vol. 2, pp. 323–328 (1982)]. En particulier le calcul révèle les régions de production négative d'énergie cinétique observées expérimentalement.

NUMERISCHE SIMULATION TURBULENTER AUFTRIEBSSTRÖMUNGEN—I. FREIE KONVEKTION AN EINER BEHEIZTEN SENKRECHTEN PLATTE

Zusammenfassung—Zwei Modelle zur Berechnung der freien Konvektion in turbulenten Strömungen bei kleinen Reynoldszahlen wurden entwickelt. Die Modelle können auch auf gemischte Konvektionsströmungen angewandt werden. Das erste, ein k, ε-Modell, basiert auf den turbulenten Transportgrößen für Impuls und Wärme. Das zweite Modell, ein algebraisches Spannungsmodell, basiert auf Näherungslösungen für die anisotropen turbulenten Ströme, die aus geeigneten Vereinfachungen der Erhaltungssätze gewonnen wurden. Beide Formulierungen sind anwendbar auf Strömungen mit variablen Eigenschaften und hohen Überhitzungsverhältnissen $\Delta T/T_\infty$ und benötigen keine Definition neuer Modellkonstanten. Kein Versuch wurde unternommen, die bekannten Werte für die Konstanten zu modifizieren, um die Übereinstimmung zwischen Messungen und Berechnungen der untersuchten Strömungen zu verbessern. Für eine solche Optimierung muß die Verfügbarkeit detaillierterer und zuverlässiger experimenteller Daten von turbulenten Größen abgewartet werden. Voll elliptische Formen der Differentialgleichungen für den Transport mit geeigneten speziellen Randbedingungen werden numerisch für zwei zweidimensionale Konfigurationen gelöst. Die erste gilt für freie Konvektion längs einer beheizten senkrechten Platte und ist Gegenstand von Teil I dieses Berichts. Die zweite gilt für freie und gemischte Konvektion von einer beheizten Vertiefung mit beliebigem rechteckigem Querschnitt und variabler Oberfläche und ist Gegenstand von Teil II. Für den Fall der senkrechten Platte zeigt ein Vergleich zwischen Messungen und Berechnungen, daß beide Modelle ziemlich genaue Ergebnisse für die mittlere Strömungsgeschwindigkeit und den mittleren Wärmeübergang liefern. Wandnahe Geschwindigkeits- und Temperaturverteilungen, berechnet mit beiden Modellen, zeigen die bekannte 1/3-Potenz Abhängigkeit.

ЧИСЛЕННОЕ ИССЛЕДОВАНИЕ ПОДЪЕМНОГО ТУРБУЛЕНТНОГО ТЕЧЕНИЯ—I. СВОБОДНАЯ КОНВЕКЦИЯ ОКОЛО НАГРЕТОЙ ВЕРТИКАЛЬНОЙ ПЛОСКОЙ ПЛАСТИНЫ

Аннотация—Предложены две модели лдя расчета свободноконвективных турбулентных течений при малых числах Рейнольдса, которые применимы также и к смешанноконвективным течениям. Первая, k–ε-модель, основана на понятии турбулентной температуропроводности для импульса и тепла. Вторая, модель алгебраического напряжения, базируется на аппроксимациях соответствующих законов сохранения для анизотропных турбулентных потоков. Обе модели применимы к потокам с переменными характеристиками и большими отношениями перегрева $\Delta T/T_\infty$ и не требуют введения новых постоянных модели. Попыток уточнения ранее предложенных значений постоянных для улучшения соответствия между экспериментальными и расчетными характеристиками исследуемого течения не предпринималось. Такое уточнение должно опираться на более детальные и надежные экспериментальные измерения характеристик турбулентности. Полные эллиптические двумерные дифференциальные уравнения переноса с заданными граничными условиями решены численно для двух видов течений. В I части исследуется свободная конвекция у нагретой вертикальной пластины. Во второй части рассматривается свободная и смешанная конвекция в нагретой полости произвольного прямоугольного сечения при различной ее ориентации. В этом случае сравнение данных измерений с результатами расчетов показывает, что обе модели дают довольно точные значения интегральных характеристик течения и теплообмена. Распределения скорости и температуры у стенки, найденные по обеим моделям, дают степенную зависимость с показателем 1/3, полученную Джорджем и Каппом [*Int. J. Heat Mass Transfer* **22,** 813–826 (1979)] и подтвержденную для температуры Сейберсом и др. [*J. Heat Transfer* **107,** 124–136 (1985)]. Значения постоянных в степенных зависимостях для скорости и температуры получены численно для больших и малых значений $\Delta T/T_\infty$. Расчеты анизотропного рейнольдсова напряжения и распределений турбулентного теплового потока качественно соответствуют измерениями Миямото и др. [*Proc. 7th Int. Heat Transfer Conference*, Vol. 2, pp. 323–328 (1982)]. В частности, с помощью расчетов точно определены наблюдаемые экспериментально области производства турбулентной кинетической энергии за счет отрицательной подъемной силы и сдвига.